

This is the accepted manuscript made available via CHORUS. The article has been published as:

Origin of First-Order-Type Electronic and Structural Transitions in IrTe_2

Kyoo Kim, Sooran Kim, K.-T. Ko, Hwangho Lee, J.-H. Park, J. J. Yang, S.-W. Cheong, and B. I. Min

Phys. Rev. Lett. **114**, 136401 — Published 31 March 2015

DOI: [10.1103/PhysRevLett.114.136401](https://doi.org/10.1103/PhysRevLett.114.136401)

The origin of first-order type electronic and structural transitions in IrTe₂

Kyoo Kim^{1,2,*}, Sooran Kim¹, K. -T. Ko^{2,3,6}, Hwangho Lee^{1,2},
J. -H. Park^{1,2,3,4}, J. J. Yang^{2,5}, S -W. Cheong^{5,7}, and B. I. Min^{1†}

¹ Department of Physics, Pohang University of Science and Technology, Pohang 790-784, Korea

² c-CCMR, Pohang University of Science and Technology, Pohang 790-784, Korea

³ MPPC-CPM, Pohang University of Science and Technology, Pohang 790-784, Korea

⁴ Division of Advanced Materials Science, Pohang University of Science and Technology, Pohang 790-784, Korea

⁵ Laboratory for Pohang Emergent Materials, Pohang University of Science and Technology, Pohang 790-784, Korea

⁶ Max Planck Institute for Chemical Physics of Solid Nöthnitzer Straße 40, D-01187, Dresden, Germany

⁷ Rutgers Center for Emergent Materials and Department of Physics & Astronomy, Piscataway, New Jersey 08854, USA

(Dated: February 25, 2015)

We have explored the origin of unusual first-order type electronic and structural transitions in IrTe₂, based on the first-principles total energy density functional theory (DFT) analysis. We have clarified that the structural transition occurs through the interplay among the charge density wave-like lattice modulation with $q_{1/5} = (1/5, 0, 1/5)$, in-plane dimer ordering, and the uniform lattice deformation. The Ir-Ir dimer formation via a molecular-orbital version of the Jahn-Teller distortion in the Ir-Ir zig-zag stripe is found to play the most important role in producing the charge disproportionation state. Angle-resolved photoemission spectroscopy reveals the characteristic features of structural transition, which are in good agreement with the DFT bands obtained by the band unfolding technique.

PACS numbers: 71.30.+h, 74.25.Jb, 71.20.-b, 71.45.Lr

A lot of recent attention has been paid to IrTe₂, since Yang *et al.*[1] and Pyon *et al.*[2] discovered superconductivity (SC) in Pd and Pt doped IrTe₂. Besides the SC in doped IrTe₂, the parent compound IrTe₂ itself exhibits quite intriguing electronic and structural properties, which has not been fully comprehended yet. IrTe₂ crystallizes in a hexagonal structure of CdI₂ type ($P\bar{3}m1$) at room temperature (T). Upon cooling, IrTe₂ undergoes a structural transition around $T_S \approx 280$ K, exhibiting a sudden jump in the resistivity with large hysteretic feature of the first-order type. It was argued that this behavior stems from the partial gap opening due to a charge density wave (CDW) transition with $q_{1/5} = (1/5, 0, 1/5)$. [1, 3] With Pd doping, the CDW is suppressed and the SC emerges with T_C up to 3 K at 4 % Pd doping. The interplay between the CDW and the SC results in a dome-like phase diagram with respect to the Pd doping ratio.

The structural transition in IrTe₂, however, looks different from a standard CDW transition. Namely, the system has the first-order type transition to a commensurate structure and exhibits the heavy reconstruction of electronic structure over large energy window.[4] The phonon softening instability signifying the structural transition was not obtained in the phonon dispersion for hexagonal IrTe₂. [8] Furthermore, unlike other transition-metal dichalcogenide systems having the SC ground state, for which the pressure suppresses the CDW structural transition but enhances the SC transition, the opposite trend was observed for IrTe₂. [5] Hence, several different scenarios have been suggested as the origin of the structural transition in IrTe₂, such as charge/orbital density wave,[1] orbital induced Peierls instability,[6, 7] crystal

field of Te p orbital,[4, 8, 9] anionic depolymerization transition.[10]

Using the single-crystal X-ray diffraction, Pascut *et al.*[11] refined the low T crystal structure of IrTe₂ as a triclinic structure ($P\bar{1}$), as shown in Fig. 1 (a). They argued that Ir dimer formation occurs during the structural phase transition, and the resulting energy gain plays a crucial role in the structural transition. In fact, IrTe₂ is a rare system that exhibits charge ordering/disproportionation together with structural modula-

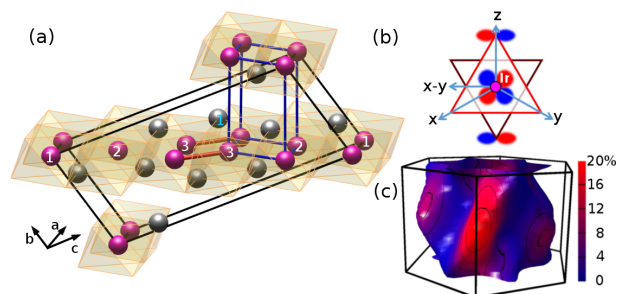


FIG. 1: (color online) (a) High T HEX unit cell (blue), and low T 5X unit cell (black) of IrTe₂. The violet (grey) spheres are Ir (Te) atoms, yellow octahedra represent IrTe₆ octahedra, and red rods indicate Ir₃-Ir₃ dimers. (b) The near E_F Ir wave function of $d_{z(x-y)}$ character forms the antibonding with Te wave functions located along diagonal directions. The bright (dark) red triangle describes the Te lattice above (below) Ir layer. x , y , and z are local coordinate of Ir, approximately pointing toward Te sites. $x-y$ lies in the Ir plane. (c) The orbital projected FS of high T phase of IrTe₂. The color of FS indicates the weight contribution from Ir $d_{z(x-y)}$, which shows the clear 1D nature.[12]

tion in the metallic state. This property suggests that IrTe₂ at low T is on the verge of localized and extended electronic system.

In this letter, we have explored the microscopic origin of the first-order type electronic and structural transitions in IrTe₂. As described above, there has been no consensus on the microscopic mechanism elucidating the first-order structural transition in IrTe₂ yet. Most of previous studies concentrated on the question which atom, Ir, or Te, is responsible for the structural transition. However, results of density functional theory (DFT) and X-ray absorption spectroscopy indicate that the Ir-Te hybridization is strong enough to yield the covalent states.[13] In this situation, separating out the Ir and Te contributions is not possible. They would contribute together to the relevant physics in IrTe₂. We have found that the first-order type electronic and structural transitions occur through the interplay among the CDW-like lattice modulation with $q_{1/5}$ (hereafter 1/5 lattice modulation), in-plane dimer ordering, and the uniform lattice deformation. We have also analyzed ARPES data for low T phase of IrTe₂ for the first time employing the band unfolding technique, and demonstrated that our structural model is quite consistent with the ARPES band dispersions, Fermi surfaces (FSs), and spectral weights.

Electronic structures within the DFT were obtained by using the full-potential linearized augmented plane wave band method implemented in Wien2k code.[14] For the structural relaxations, both the pseudopotential band method implemented in VASP code[15] and the Wien2k were employed. We optimized the hexagonal structure with the inclusion of the spin-orbit coupling, utilizing three exchange-correlation potentials: local density approximation (LDA), generalized gradient approximation (GGA) in the PBE and PBEsol schemes.[16] Since the PBEsol gives the optimized volume closest to experimental one, we chose the PBEsol results through out this paper.[17]

Figure 1(c) shows the DFT FS of high T phase of IrTe₂. The color indicates the weight contribution from the Ir $d_{z(x-y)}$ orbital character, the wave function form of which is depicted in Fig. 1(b). This orbital projected FS manifests that the FS has quasi-one-dimensional (1D) nature along three different diagonal directions. The 1D nature of the FS is more clearly seen in the tight binding (TB) model analysis in the supplement.[18] Indeed, this 1D-ness together with saddle point scattering produces the FS nesting and the corresponding susceptibility peak along the diagonal direction.[1] Even though the susceptibility peak itself is not fully sufficient to explain the first-order structural transition of IrTe₂, it is to be an important ingredient for the 1/5 modulation observed for low T phase of IrTe₂. Hereafter, we will refer to high and low T phases of IrTe₂ as HEX and 5X, respectively.

We have first examined the energetics between the HEX and 5X phases of IrTe₂. The relaxed 5X structure

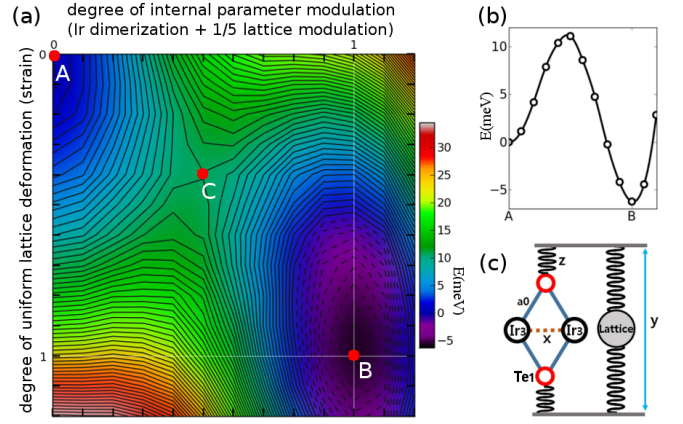


FIG. 2: (color online) (a) Energy contour of IrTe₂ in the structural phase space. A and B stand for the structural parameters of HEX5 and 5X, respectively. The horizontal and vertical axes represent the in-plane dimerization coupled to the 1/5 lattice modulation and the uniform lattice deformation, respectively, which are linearly interpolated between structural parameters of A and B on 13×13 mesh points.[18, 29] Energy zero corresponds to the energy of the HEX5 structure. C represents a saddle point where the energy barrier is the lowest. (b) Energy profile along the path connecting A and B directly. The 5X structure is seen to be lower in energy than the HEX5 by 6.25 meV per formula unit. (c) A schematic mechanical model describing the interplay between the Ir₃-Ir₃ dimerization (x) and the uniform lattice deformation (y), which are coupled through Te₁ distortion (z).[18]

was obtained starting from the experimental 5X structure refined by Pascut *et al.*[11] To compare total energies under the same condition, we considered a supercell of high T phase of IrTe₂ (HEX5), which is described with the same group symmetry as for 5X IrTe₂. It is expected that the structural transition occurs through the uniform lattice deformation (changes of lattice constants and angles between them) and the modulation of internal degrees of freedom (the 1/5 lattice modulation and the Ir dimerization). So, to separate out effects of the lattice deformation and the modulation, we considered artificial structural phase space in-between the HEX5 and 5X structures, which was obtained by linearly interpolating the lattice structures and the internal parameters (atomic positions) of HEX5 and 5X phases independently. Total energy calculations were performed on this simplified structural phase space, by using the Wien2k.

The energy contour in Fig. 2(a) shows that there are two energy minima in the structural phase space, which correspond to HEX5 and 5X structures. The energy of the 5X phase is lower than that of the HEX5 by 6.25 meV per formula unit. The double well structure with a saddle-shaped barrier in-between two minima indicates an existence of the first-order type structural transition. As shown in Fig. 2(b), the height of energy barrier is about 11 meV per formula unit. It has been suggested that the in-plane Ir dimerization plays a crucial role in

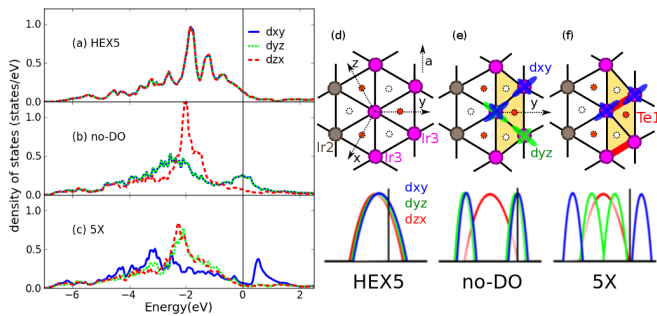


FIG. 3: (color online) (a)-(c) Partial DOSs for HEX5, no-DO, and 5X structures, where no-DO corresponds to an artificial structure without dimer ordering, as depicted in (e). (d)-(f) In-plane structures and corresponding schematic DOSs for HEX5, no-DO, and 5X. Yellow shade represents the compressed region due to the $1/5$ lattice modulation. Large (small) circles denote Ir (Te) atoms. The red and white small circles are Te atoms located above and below Ir layer. Te atoms in the yellow shade are Te_1 . Two DOS peaks in blue and green correspond to bonding/antibonding states of d_{xy} and d_{yz} . Note that d_{xy} and d_{yz} orbitals participate in two different dimer orderings. One specific dimer ordering (red thick lines) is shown in (f), which is associated with the d_{xy} orbital.

stabilizing the 5X structure.[11, 19, 20] Figure 2(a), however, reveals that just the Ir dimer formation, which corresponds to the increment along the horizontal axis from A, increases the energy solely monotonically. Rather it reveals that not only the in-plane Ir dimerization but also the lattice deformation is an essential ingredient for the structural transition to 5X. This explains why there is no softening feature in the phonon dispersion for HEX IrTe_2 , which does not take into account the uniform lattice deformation.[8]

The Ir dimerization pushes away nearby Te_1 atoms, which brings about the lattice deformation. This mechanism can be schematically described by a simple mechanical model in Fig. 2(c), which contains the attractive interaction between Ir dimers and the additional harmonic interactions describing the lattice deformation. It shows that, as x decreases with dimerization, Te_1 is pushed away from Ir_3 , and so y increases due to the spring z . This model yields the double-well energy minima properly, as shown in the supplement.[18] It is thus deduced that the interplay among the $1/5$ lattice modulation, the in-plane Ir dimerization, and the uniform lattice deformation is the origin of the first-order structural transition in IrTe_2 . Pascut *et al.*[11] performed the similar energy calculations for HEX5 and 5X phases, but they got the lower energy for HEX5 than for 5X, as opposed to Fig. 2(b). Presumably, their unphysical result comes from the less precise description of structural parameters by using the different exchange-correlation functional.

It is worthwhile to note that the direction of the $1/5$ lattice modulation and the direction of the in-plane dimer

formation do not coincide. Moreover there are two substructures depending on the Ir_3 - Ir_3 dimer ordering patterns along the a direction (see Fig. 3). We expect that this feature arises from the cooperative Jahn-Teller (JT) type distortion that occurs with the $1/5$ lattice modulation. In Fig. 3, we constructed an artificial structure with no dimer ordering (no-DO), lattice constants and atomic positions of which are identical to those of HEX5 except for Ir_3 and Te_1 positions. In fact, the no-DO phase results from the $1/5$ lattice modulation. As shown in Fig. 3(e), in no-DO, Ir_3 - Ir_3 dimer ordering is not realized yet, but Ir_3 - Ir_3 distance becomes shorter uniformly and the Te_1 atoms moved farther from the Ir layer, forming a Ir_3 zigzag chain along the a direction. In HEX5, the densities of states (DOSs) for three t_{2g} orbitals are degenerate, as shown in Fig. 3(d). But, as the $1/5$ lattice modulation occurs, the degeneracy of t_{2g} orbitals is lifted, separating out d_{zx} orbital, which has weaker hopping in the in-plane zigzag chain.

Notice that the charge transfer to the Te_1 p orbital occurs in this process,[6, 11, 13] resulting in the increase of hole carriers in the degenerate antibonding Ir_3 - Ir_3 d_{xy}/d_{yz} molecular orbitals. These two degenerate orbitals, which belong to different molecules as depicted in Fig. 3(e), couple to two modulations in the Ir_3 zig-zag chain, leading to a specific dimer ordering, as shown in Fig. 3(f). This is a molecular-orbital version of the JT effect in the zig-zag stripe comprised of Ir_3 and Te_1 atoms. As a consequence of the dimer ordering, Te_1 moves away from Ir_3 - Ir_3 center, and thereby Ir_3 dimerization induces the uniform lattice deformation, as described in Fig. 2(c), giving rise to the first-order structural transition. Although we describe the process in sequence, they would occur simultaneously.

There are experimental evidences for charge disproportionation/ordering of Ir ($3+/4+$) in IrTe_2 . [6, 10, 22, 23] To inspect the charge disproportionation property in the 5X phase of IrTe_2 , we counted the number of Ir d (t_{2g}) electrons inside the muffin-tin sphere. Table I shows that Ir_3 has less electrons than Ir_1 and Ir_2 , by about 0.5 electrons, reflecting that the valence state of Ir_3 is close to $4+$, while those of Ir_1 and Ir_2 close to $3+$. Table I also presents the core level shift of Ir $4f$ levels in the 5X phase with respect to that in the HEX phase. The $4f$ level in

TABLE I: Ir $5d$ t_{2g} orbital occupation n and Ir $4f_{7/2}$ core level shift ΔE in the 5X phase with respect to that in the HEX phase of IrTe_2 .

Ir type	n [Ir $5d$ t_{2g}]	ΔE [Ir $4f$] (eV)
Ir_1	4.49	0.040
Ir_2	4.48	-0.057
Ir_3	3.97	-0.432

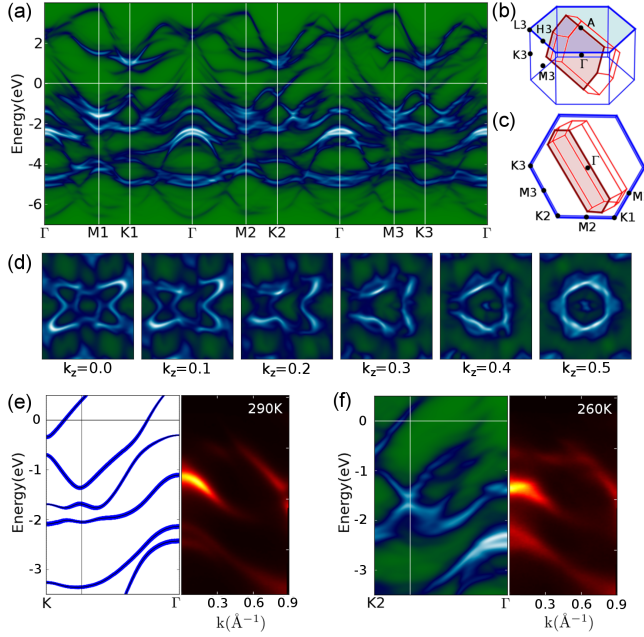


FIG. 4: (color online) (a) The DFT band structure of 5X IrTe₂ unfolded into the HEX BZ. The intensity of band dispersion represents the weight of Ir-projected character. (b) The relation between the large HEX and the small 5X BZ. (c) The Γ ($k_z = 0$) plane of the HEX BZ. (d) The DFT FSs of 5X IrTe₂ unfolded into the HEX BZ for different k_z . (e) The DFT bands calculated for the HEX structure (left) are compared with ARPES data (right) at $T = 290$ K above T_S . (f) The unfolded DFT bands for the 5X structure (left) are compared with ARPES data (right) at $T = 260$ K below T_S . The vertical lines in the DFT bands represent the experimental scan range (0.9 \AA). Photon energy used in this ARPES is 75.0 eV .

Ir₃ is deeper than those in Ir₁ and Ir₂ by about 0.4 eV , which indicates less screening of nuclear potential due to less number of valence electrons in Ir₃ than others. These values are consistent with experimental findings by Qian *et al.*[9] The properties in Table I show strong indication of charge disproportionation feature in the 5X phase of IrTe₂, which indeed arises from the Ir₃-Ir₃ dimerization.

To examine how the structural transition and the dimer formation are reflected in the electronic structure of the 5X structure, we compared the DFT band dispersions with ARPES data in Fig. 4.[18] For this purpose, we have utilized the band unfolding technique,[24–27] which takes into account the Bloch phase factor between 5X and HEX cells, and maps the wave function in 5X cell to that in HEX cell. The relation between the HEX and the 5X Brillouin-zone (BZ) is shown in Fig. 4(b) and (c).[18] Figure 4(a) presents Ir-projected band dispersions of 5X that are unfolded into a hexagonal in-plane BZ along k -path in Fig. 4(c).

The photoionization cross section of Ir $5d$ is 11 times stronger than Te $5p$ at 75 eV . [28] So we considered Ir-projected bands in Fig. 4(a).[18] It is seen that the band

splittings appear at some k -points near E_F . For example, there appears an abrupt change/splitting in the near- E_F band along $K1-\Gamma$, which is quite different from that along $K2-\Gamma$. Another noticeable feature is the appearance of flat bands around -1.4 eV near Γ (see along $K2-\Gamma-M3$). According to our TB model analysis along the in-plane Ir chain, this unique dispersion comes from the different on-site energy term of dimerized Ir₃ from those of other Ir atoms, which happens due to the charge transfer and/or the crystal field effect (see supplement).[18]

In Fig. 4(d), unfolded 5X FSs are plotted in the HEX BZ for various k_z cuts. For $k_z = 0$, one of the lobes in outer FS almost disappears. It is due to the gap opening in this part of the FS of 5X. Note that this gap opens not by the $1/5$ lattice modulation but by the lifting of orbital degeneracy due to the JT distortion (see Fig. 3(f)). In actual ARPES data, however, the gap opening at one of outer FS lobes is not clearly observed. Instead, the reduction of ARPES intensity is observed at all the outer FS regime for 5X with respect to that for HEX. It is because of the existence of three types of domains, which yields the domain averaged ARPES intensity.[18]

Figures 4(e) and (f) provide the comparison of DFT band structures and ARPES data. In Fig. 4(e), ARPES data measured at $T = 290 \text{ K}$ are compared with DFT bands of HEX, while, in Fig. 4(f), those at $T = 260 \text{ K}$ are compared with DFT unfolded bands of 5X. Quite good agreements in the spectral weights as well as the dispersions are revealed at both T 's, which indeed verifies the formation of Ir₃ dimer ordering upon cooling. Furthermore, it supports the reliability of the structural data employed in this study.[11]

Finally, it is worthwhile to examine the doping and pressure effects on the structural and SC transitions in IrTe₂ based on the present model. We have found that, under the positive pressure, the peak structure in the susceptibility $\chi(q)$ of HEX IrTe₂ becomes enhanced at $q_{1/5}$, while, under the negative pressure, that becomes reduced. The reduction in the peak structure of $\chi(q)$ is also obtained when considering the carrier doping of Pd and Pt and associated structural relaxations. Even though more detailed study is needed, this feature provides qualitative clarification of the intriguing pressure effects on the structural and SC transitions in IrTe₂, [5] and also the doping-induced SC transition in doped IrTe₂. [2, 21] The c/a ratio as well as the internal structural parameters will strongly depend on the pressure. In fact, the angle between atoms in the Ir-Te-Te-Ir chain is found to be changed sensitively with varying the pressure. Then the 1D-ness in IrTe₂, which is essential ingredient of the structural transition, is to be altered, and accordingly to induce the SC transition.

In conclusion, we have demonstrated that there is an energy barrier in-between the high T (HEX5) and low T (5X) phases of IrTe₂, which explains the first-order type electronic and structural transitions in IrTe₂. This

feature explains the limitation of linear response-based calculations, such as phonon calculation, in describing the structural transition in IrTe₂. We have clarified that the structural transition in IrTe₂ originates from the interplay among the CDW-like lattice modulation with $q_{1/5} = (1/5, 0, 1/5)$, the in-plane Ir₃-Ir₃ dimer formation, and the uniform lattice deformation, all of which are coupled through the molecular-orbital version of the JT distortion. With Ir₃-Ir₃ dimerization, the charge disproportionation state is realized. Quite good agreement between the unfolded DFT bands and FSs and the ARPES data for both HEX and 5X phases of IrTe₂ supports our analysis of the structural transition, especially the formation of Ir₃-Ir₃ dimerized states.

This work was supported by the NRF (No. 2009-0079947 and No. 2011-0025237), the POSTECH BSRI Grant, and KISTI (No. KSC-2013-C3-064). KT was supported by the Max Planck-POSTECH Center for Complex Phase Materials (No. KR2011-0031558). JHP was supported by the National Creative Initiative (No. 2009-0081576) and Max Plank POSTECH/KOREA Research Initiative (No. 2011-0031558). SWC was also supported by the NSF (No. NSF-DMFEF-1233349). Fruitful discussions with Beom Hyun Kim, Jun Sung Kim, and Han Woong Yeom are greatly appreciated.

* kyoo@postech.ac.kr

† bimin@postech.ac.kr

- [1] J. J. Yang, Y. J. Choi, Y. S. Oh, A. Hogan, Y. Horibe, K. Kim, B. I. Min, and S.-W. Cheong, Phys. Rev. Lett. **108**, 116402 (2012).
- [2] S. Pyon, K. Kudo, and M. Nohara, J. Phys. Soc. Jpn. **81**, 053701 (2012).
- [3] $(1/5, 0, 1/5)$ and $(1/5, 0, -1/5)$ are the same considering the different crystal orientation. The relative angle between them is 30°.
- [4] A. F. Fang, G. Xu, T. Dong, P. Zheng, and N. L. Wang, Sci. Rep. **3** 1153, (2013).
- [5] A. Kiswandhi, J. S. Brooks, H. B. Cao, J. Q. Yan, D. Mandrus, Z. Jiang, and H. D. Zhou, Phys. Rev. B **87**, 121107 (2013).
- [6] D. Ootsuki, Y. Wakisaka, S. Pyon, K. Kudo, M. Nohara, M. Arita, H. Anzai, H. Namatame, M. Taniguchi, N. L. Saini, and T. Mizokawa, Phys. Rev. B **86**, 014519 (2012); Journal of Physics: Conference Series **428**, 012018 (2013).
- [7] D. Ootsuki, S. Pyon, K. Kudo, M. Nohara, M. Horio, T. Yoshida, A. Fujimori, M. Arita, H. Anzai, H. Namatame, M. Taniguchi, N. L. Saini, and T. Mizokawa, J. Phys. Soc. Jpn. **82**, 093704 (2013).
- [8] H. Cao, B. C. Chakumakos, X. Chen, J. Yan, M. A. McGuire, H. Yang, R. Custelcean, H. Zhou, D. J. Singh, and D. Mandrus, Phys. Rev. B **88**, 115122 (2013).
- [9] T. Qian, H. Miao, Z. J. Wang, X. Shi, Y. B. Huang, P. Zhang, N. Xu, L. K. Zeng, P. Richard, M. Shi, G. Xu, X. Dai, Z. Fang, A. F. Fang, N. L. Wang, and H. Ding, New J. Phys. **16**, 123038 (2014).
- [10] Y. S. Oh, J. J. Yang, Y. Horibe, and S.-W. Cheong, Phys. Rev. Lett. **110**, 127209 (2013).
- [11] G. L. Pascut, K. Haule, M. J. Gutmann, S. A. Barnett, A. Bombardi, S. Artyukhin, T. Birol, D. Vanderbilt, J. J. Yang, S.-W. Cheong, and V. Kiryukhin Phys. Rev. Lett. **112**, 086402 (2014).
- [12] To plot orbital projected FS, we used *moliso* package; C. B. Hübschle, and P. Luger, J. Appl. Cryst. **39**, 901 (2006).
- [13] K. Takubo, R. Comin, D. Ootsuki, T. Mizokawa, H. Wadati, Y. Takahashi, G. Shibata, A. Fujimori, R. Sutarto, F. He, S. Pyon, K. Kudo, M. Nohara, G. Levy, I. S. Elfimov, G. A. Sawatzky, and A. Damascelli, Phys. Rev. B **90**, 081104(R) (2014).
- [14] P. Blaha, K. Schwarz, G.K.H. Madsen, D. Kvasnicka, J. Luitz, WIEN2k, An Augmented Plane Wave + Local Orbitals Program for Calculating Crystal Properties, Karlheinz Schwarz, Techn. Universität Wien, Austria, (2001), ISBN 3-9501031-1-2.
- [15] G. Kresse and J. Furthmüller, Phys. Rev. B **54**, 11169 (1996); Comput. Mater. Sci. **6**, 15 (1996).
- [16] J. P. Perdew, A. Ruzsinszky, G. I. Csonka, O. A. Vydrov, G. E. Scuseria, L. A. Constantin, X. Zhou, and K. Burke, Phys. Rev. Lett. **100**, 136406 (2008).
- [17] The LDA and PBE give 1.5 % smaller and 2.0 % larger volumes than the experimental volume, while the PBEsol gives only slightly larger (0.5 %) volume.
- [18] See the Supplemental Materials, which include Refs. [30–32], for the model TB analysis to describe a quasi-1D FS, the effect of the charge disproportionation on the band dispersion, the mechanical model describing the dimer formation and the associated lattice deformation, the full unfolded bands at the Γ and A planes, the relation between BZs, the detailed descriptions on structures and ARPES experiments.
- [19] T. Toriyama, M. Kobori, T. Konishi, Y. Ohta, K. Sugimoto, J. Kim, A. Fujiwara, S. Pyon, K. Kudo, and M. Nohara, J. of Phys. Soc. Jpn. **83**, 033701 (2014).
- [20] B. Joseph, M. Bendele, L. Simonelli, L. Maugeri, S. Pyon, K. Kudo, M. Nohara, T. Mizokawa, and N. L. Saini, Phys. Rev. B **88**, 224109 (2013).
- [21] K. Kudo, M. Kobayashi, S. Pyon, and M. Nohara, J. Phys. Soc. Jpn. **82**, 085001 (2013).
- [22] S. Jobic, R. Brec, and J. Rouxel, J. Solid State Chem. **96**, 169 (1992).
- [23] K. Mizuno, K. Magishi, Y. Shinonome, T. Saito, K. Koyama, N. Matsumoto, and S. Nagata, Physica B, **312-313**, 818, (2002).
- [24] W. Ku, T. Berlijn, and C.-C. Lee, Phys. Rev. Lett. **104**, 216401 (2010).
- [25] We have used Wannierized Löwdin orbitals from 110 bands in the energy window from -7.0 eV to 4.0 eV: $5 \times (10 \text{ Ir } 5d \text{ orbitals}) + 2 \times (6 \text{ Te } 5p \text{ orbitals})$.
- [26] J. -S. Kang, D. H. Kim, H. J. Lee, J. H. Hwang, H. G. Lee, H. -D. Kim, B. H. Min, K. E. Lee, Y. S. Kwon, J. W. Kim, Kyoo Kim, B. H. Kim, and B. I. Min, Phys. Rev. B **85**, 085104 (2012).
- [27] H. J. Noh, J. Jeong, B. Chang, D. Jeong, H. S. Moon, E. J. Cho, J. M. Oh, J. S. Kim, K. Kim, B. I. Min, H. K. Lee, J. Y. Kim, B. G. Park, H. D. Kim, and S. Lee, Sci. Rep. **4**, 3680 (2013).
- [28] J. J. Yeh, *Atomic Calculation of Photoionization Cross-Sections and Asymmetry Parameters* (Gordon and Breach, New York, 1993).

- [29] Nudged elastic band calculation can be the alternative to simulate such energy barrier; G. Henkelman, B. P. Uberuaga, H. Jonsson, J. Chem. Phys. **113**, 9901 (2000).
- [30] M. H. Whangbo, E. Canadell, P. Foury, and J. P. Pouget, Science **252**, 96 (1991).
- [31] T. M. Rice, and G. K. Scott, Phys. Rev. Lett **35**, 120 (1975).
- [32] J.-H. Xu, T. J. Watson-Yang, J. Yu, and A. J. Freeman Phys. Lett. A **120**, 489 (1987).